Nuclear fusion during yeast mating occurs by a three-step pathway

Patricia Melloy,[1,3] Shu Shen,[1] Erin White,[2] J. Richard McIntosh,[2] and Mark D. Rose[1]

[1]Department of Molecular Biology, Princeton University, Princeton, NJ 08544
[2]Mollecular, Cellular, and Developmental Biology, University of Colorado at Boulder, Boulder, CO 80309
[3]Department of Biological and Allied Health Sciences, Fairleigh Dickinson University, Madison, NJ 07940

I n *Saccharomyces cerevisiae*, mating culminates in nuclear fusion to produce a diploid zygote. Two models for nuclear fusion have been proposed: a one-step model in which the outer and inner nuclear membranes and the spindle pole bodies (SPBs) fuse simultaneously and a three-step model in which the three events occur separately. To differentiate between these models, we used electron tomography and time-lapse light microscopy of early stage wild-type zygotes. We observe two distinct SPBs in ∼80% of zygotes that contain fused nuclei, whereas we only see fused or partially fused SPBs in zygotes in which the site of nuclear envelope (NE) fusion is already dilated. This demonstrates that SPB fusion occurs after NE fusion. Time-lapse microscopy of zygotes containing fluorescent protein tags that localize to either the NE lumen or the nucleoplasm demonstrates that outer membrane fusion precedes inner membrane fusion. We conclude that nuclear fusion occurs by a three-step pathway.

Introduction

Cell fusion is a fundamental process in the biology of eukaryotic cells; it is essential for fertilization and occurs at key times during somatic development (White and Rose, 2001; Chen and Olson, 2005; Ogle et al., 2005). Yeast conjugation, or mating, can be divided into five broad steps: cell to cell signaling, cell polarization, cell fusion, nuclear congression, and nuclear fusion (Sprague and Thorner, 1992; Rose, 1996; Marsh and Rose, 1997). Mating begins when two cells of the opposite mating type respond to the pheromones released by a nearby prospective mating partner. The cells repolarize to form shmoos; that is, each cell forms a projection with its apical end directed toward the prospective mating partner. The two cells adhere at the shmoo tips to form a prezygote. Degradation of the cell wall and fusion of the plasma membranes allow the cells to fuse, providing continuity of the two formerly separate cytoplasms. Finally, the nuclei congress in a microtubule-dependent manner (Molk et al., 2006), and the nuclear envelopes (NEs) fuse to produce a single diploid nucleus (Rose, 1991, 1996).

Like other fungi, *Saccharomyces cerevisiae* undergoes cell division and mating without NE breakdown (Byers, 1981a). Therefore, NE fusion is essential for the production of a diploid

nucleus. However, the pathway controlling NE fusion is not well understood. Yeast NE fusion is a homotypic reaction in that both membranes correspond to the same subcellular compartment. However, nuclear fusion is inherently more complex than viral membrane fusion because it entails the fusion of two pairs of membrane bilayers. Therefore, it is analogous to the fusion of other organelles (Catlett and Weisman, 2000; Meeusen et al., 2004; Okamoto and Shaw, 2005). Like mitochondrial fusion, NE fusion requires the alignment and fusion of both inner and outer membranes.

Yeast karyogamy or *kar* mutants are defective in nuclear fusion and can be divided into two major categories. Type I mutants display defects in nuclear congression in that the nuclei fail to move together and typically exhibit defects in the cytoplasmic microtubules (Kurihara et al., 1994; Rose, 1996; Gammie and Rose, 2002). In type II mutant zygotes, the nuclei become closely apposed yet remain unfused (Kurihara et al., 1994). In certain class II karyogamy mutants, the apposed nuclei appear to be connected by membrane bridges that run between the outer nuclear membranes (Beh et al., 1997; Brizzio et al., 1999). Both of these classes of karyogamy mutants typically progress into mitosis, yielding haploid progeny.

All of the proteins known to be required for nuclear membrane fusion (e.g., Kar2p, Kar5p, Kar7p/Sec71p, Kar8p/Jem1p, and Prm3p) are localized to the NE (Rose et al., 1989; Latterich and Schekman, 1994; Beh et al., 1997; Brizzio et al., 1999; Beilharz et al., 2003). However, one of the mysteries of NE fusion is

that many of the requisite proteins reside within the NE lumen, where it is unlikely that they could play a direct role in the initial stages of membrane fusion. Nevertheless, the genetic data are supported by in vitro fusion experiments that indicate a role for the luminal proteins Kar2p, Kar5p, and Kar8p/Jem1p in the overall fusion process (Kurihara et al., 1994; Latterich and Schekman, 1994). To date, it has been difficult to define the role of these proteins, although their roles may be similar to functions that they are already known to perform in the ER (Rose et al., 1989; Ng and Walter, 1996; Nishikawa and Endo, 1997; Brizzio et al., 1999; Nishikawa et al., 2001).

The yeast microtubule-organizing center, the spindle pole body (SPB), is critical to both nuclear congression and nuclear membrane fusion (for review see Jaspersen and Winey, 2004). The cytoplasmic microtubules that bring the two nuclei together during congression are nucleated from the half-bridge of the SPB (Byers, 1981a). Several type I karyogamy mutants have defects in SPB-associated proteins, including Kar1p and Mps3p (Rose and Fink, 1987; Nishikawa et al., 2003; for review see Jaspersen and Winey, 2004). During NE fusion, the SPBs are thought to dictate the initial site of membrane fusion (Byers and Goetsch, 1975). However, the steps of membrane fusion have remained unclear. Two models have been proposed to describe these steps (Fig. 1; Rose, 1996). In the one-step model, membrane fusion occurs at the SPB, at whose margins the inner and outer membranes are continuous. Such fusion could allow the inner and outer nuclear membranes to fuse simultaneously. In the alternative model, nuclear fusion occurs in three separate steps. First, the outer membranes fuse, allowing the contents of the NE lumens to become continuous. Next, the inner membranes fuse, allowing continuity of the nuclear contents. Finally, the SPBs fuse within the plane of the membrane. Early electron microscopy studies supported the one-step model, with nuclear membrane and SPB fusion occurring simultaneously (Byers and Goetsch, 1974, 1975; Byers, 1981a; for review see Jaspersen and Winey, 2004). However, the luminal localization of proteins required for karyogamy, such as Kar2p, was difficult to reconcile with the one-step model.

We have used two experimental approaches to determine whether nuclear fusion during mating occurs via one or three steps. First, electron tomography (ET) was conducted on fixed wild-type zygotes at different stages of nuclear fusion. ET is superior to serial section electron microscopy for the reconstruction of spatial details in three dimensions in several ways (O'Toole et al., 2002). First, it allows the examination of thick slices of a cellular sample, provides images with essentially isotropic resolution at 4–6 nm, and allows a flexible analysis of 3D structures. Second, live cell time-lapse microscopy was conducted on zygotes tagged with fluorescent protein markers for each relevant compartment to map the stages of nuclear fusion. Live cell fluorescence microscopy lacks the spatial resolution to visualize SPB fusion but, in contrast to static electron microscopy, allows direct determination of the temporal order of events. Thus, the two approaches complement one another. Collectively, our data show that nuclear fusion occurs by three distinct steps: outer membrane fusion, inner membrane fusion, and SPB fusion.
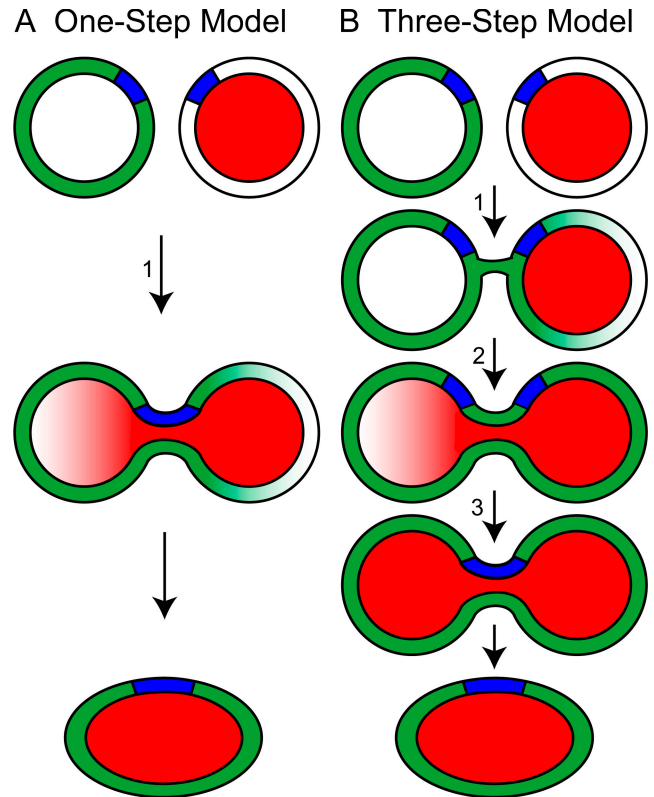

Figure 1. **The three-step versus one-step models of nuclear fusion.** A schematic diagram of the one-step versus three-step models of yeast nuclear fusion. (A) In the one-step model, NE fusion occurs in a single concerted reaction at the edge of the SPB, where the inner and outer NEs are continuous. (B) In the three-step model, outer NE fusion (1) precedes inner NE fusion (2), which precedes SPB fusion (3). To distinguish between the models, the two separate compartments (lumen of the NE and the nucleoplasm) were prelabeled with different fluorescent proteins (GFP for the NE lumen, green vs. RFP or mCherry marker for the nucleoplasm; red). If the three-step model is correct, we expect to detect transfer of the NE lumenal marker to the mating partner before transfer of the nucleoplasm marker. SPB (blue) fusion would occur at a later step. Intermediates with two distinct SPBs in a single fused nucleus should be observed. If the one-step model is correct, both the NE lumenal marker and the nucleoplasm marker should initiate transfer at the same time, and no intermediates would be detected.

Results

ET of wild-type zygotes at different stages of nuclear fusion

Although the general stages of cell fusion and karyogamy have previously been described by electron microscopy (Byers, 1981a; Gammie et al., 1998), specific intermediates of nuclear fusion were not well characterized. Therefore, we elected to use ET to provide a more detailed examination of the outer and inner NE, the SPBs, and cytoplasmic microtubules during nuclear fusion.

Nuclear congression and membrane fusion occur within 10–15 min after cell fusion, making it difficult to capture intermediates in nuclear fusion (Maddox et al., 1999; and our unpublished data). To identify zygotes at the appropriate stage of mating just before and during membrane fusion, we scanned populations of mating cells by light microscopy to identify times at which a large fraction of the cells was at an appropriate stage of conjugation. These populations were cryoimmobilized with a high pressure freezer, fixed by freeze substitution,

embedded in plastic, and serially sectioned for examination by ET (see Materials and methods). Individual sections were scanned at low magnification to identify zygotes that were parallel to the plane of sectioning and that had a narrow zone of cell fusion (measured orthogonal to the long axis of the zygote), which indicated that cell fusion had occurred just before freezing. Such cells were found with a frequency of roughly one in 1,000. In this population, we identified zygotes in which the NEs were unfused, in which NEs were partially fused, in which NE fusion had been completed, and at several stages of SPB fusion (see Figs. 2–4). Tomograms of 22 wild-type zygotes were analyzed (Table S1; available at http://www.jcb.org/cgi/content/full/jcb .200706151/DC1). In some cases, it was possible to reconstruct two or three serial semithick sections, which provided 0.5–1 μm of sample thickness and an area of ∼2 × 4 μm in the section plane. From these 3D image data, models highlighting the relevant cellular structures (outer and inner NE, SPBs, and microtubules) were generated.

A representative model of a zygote, which had completed cell and NE fusion, is shown in Fig. 2, with all structures indicated (see the tomographic slice in A and the model in D; also see Video 1, available at http://www.jcb.org/cgi/content/full/jcb .200706151/DC1). Microtubules (Fig. 2 D, yellow) were traced from their point of nucleation near the SPB either to their true end or until they left the reconstructed volume (Fig. 2, C and D). The margins of the SPBs were traced in pink. Outer and inner nuclear membranes were traced on every fourth tomographic slice along the z axis, an interval of 4–5 nm (Fig. 2, D and E; green and blue, respectively). After the major cellular structures had been traced, IMOD software was used to mesh the outlines, providing a 3D rendering of the modeled objects (O'Toole et al., 2002). In the example shown in Fig. 2 D, the cell walls and plasma membrane (purple) were continuous, indicating that cell fusion had been completed. The nuclei were joined by continuous inner and outer nuclear membranes (Fig. 2, B and E; blue and green, respectively), indicating that NE fusion had been completed. Cell fusion had occurred recently in this zygote, as indicated by the presence of vesicles near the zone of cell fusion (Fig. 2 D, red). In addition, the zone of cell fusion and region of nuclear fusion were both very narrow. Both regions expand as the zygotes mature (Gammie et al., 1998). Often the NEs appeared to be stretched out in zygotes in which nuclear fusion had not advanced far beyond the initial stages. The stretched appearance may reflect random movement of the nuclei and tension on the NEs. In Fig. 2, the stretching appeared asymmetric; however, in other zygotes, stretching was more symmetric (Fig. 3 B).

Outer NE fusion precedes inner NE fusion; membrane fusion precedes SPB fusion

The proximity of the nuclei, the morphology of the membranes, the position of the SPBs, and the width of the region of nuclear fusion (if present) were all used to order the zygotes along a presumed pathway of nuclear fusion. Tomograms were carefully examined to determine whether outer membrane fusion, inner membrane fusion, and SPB fusion had occurred. In a representative tomogram of a mating pair that had completed cell
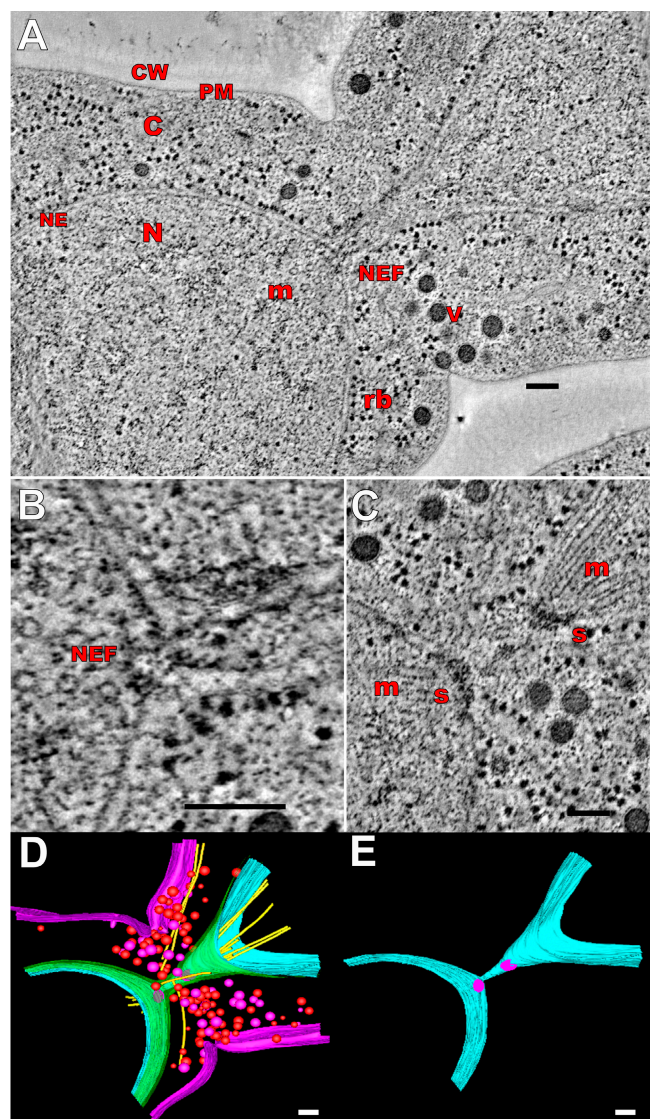

Figure 2. **Nuclear membrane fusion precedes SPB fusion in wild-type mating cells as visualized by ET.** (A) A representative tomographic slice of a zygote fixed at an early stage of NE fusion. (B) A magnified view of the region of NE membrane fusion. Note that the image in B is rotated ∼20° clockwise relative to A. (C) A magnified view of the SPBs in the zygote depicted in A. The image is from a different tomographic slice than in A. (D) The model corresponding to the tomographic slice shown in A, highlighting various cellular structures. Structures modeled include the outer NE (green), inner NE (light blue), SPB central plaques (pink), microtubules (yellow), plasma membrane (purple), and vesicles (pink and red spheres). (E) The same model displaying only the inner NE and the central plaques of the SPB. C, cytoplasm; CW, cell wall; m, microtubule; N, nucleus; NE, nuclear envelope; NEF, region of NE fusion; PM, plasma membrane; rb, ribosome; s, SPB; v, vesicle. Bars, 100 nm.

fusion but not yet initiated nuclear fusion (Fig. 3 A), one can see two nuclei with both outer and inner membranes still separate (Fig. 3 A, green and blue, respectively). Note the elongated shapes of the nuclei, which narrow to a rounded point in the region closest to one another. Electron-dense material is visible at the tips of both nuclei. On either side of the forward edges of the nuclei are the SPBs embedded in the NE (Fig. 3 A, pink disks). The dark-stained layers extending from the margins of the SPBs over the forward edges of the nuclei are the half-bridges.
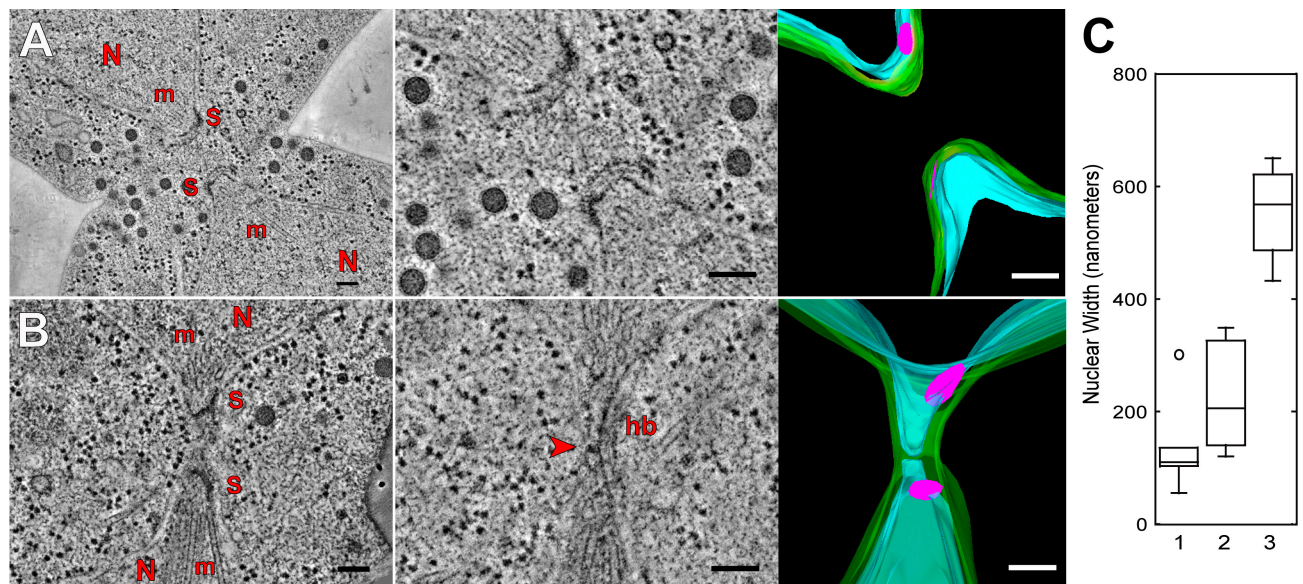
Figure 3. **NE fusion occurs in multiple steps in wild-type cells.** (A and B) Tomograms depicting zygotes before (A) and during (B) NE fusion. (A) A slice through a tomogram of wild-type mating in which cell fusion but not nuclear fusion has occurred. The left panel shows a low magnification of the zygote, the middle panel shows a magnified view of the SPBs, and the right panel shows a model highlighting the details of the SPBs and nuclear membranes. The two SPB half-bridges are on the leading edge of the NEs, with central plaques on either side. (B) A zygote in which outer nuclear membrane fusion has occurred but not inner membrane fusion. The left panel shows a slice through the two SPBs, and the middle panel shows a slice deeper in the tomogram through the central region of membrane fusion. The closely apposed but unfused inner NEs are indicated by an arrowhead. On the right side of the NEs are the half-bridges extending from the SPBs, which are not visible in this slice. The NEs on the left side were more visible in other slices. The corresponding model has been rotated about the x axis to show the gap between the two inner membranes. hb, half-bridge; m, microtubule; N, nucleus; s, SPB. In the model images, the SPB central plaques (pink) and the outer and inner NEs (green and light blue, respectively) are indicated. (C) SPB fusion occurs after partial dilation of the nuclear fusion pore. Graphs plotting the width of the nucleus across the narrowest constriction, measured from the outer edge of the NEs, in different classes of zygotes. 1, after membrane fusion but before SPB fusion ($n = 8$); 2, after initiation of half-bridge fusion ($n = 8$); and 3, partially or completely fused SPB central plaques ($n = 4$). Bars, 100 nm.

Cytoplasmic microtubules were observed connecting the two SPBs but have been omitted from the models for clarity. Vesicles clustered near the remnant cell walls at the zone of cell fusion indicate that cell fusion had occurred recently in this zygote.

In 21 of our 22 tomograms, NE fusion had been initiated or completed. One tomogram appeared to capture a particularly interesting intermediate in NE fusion (Fig. 3 B). Although the SPBs were unfused (Fig. 3 B, left), a different tomographic slice showed that the outer nuclear membranes were continuous (Fig. 3 B, middle; green in model). Close examination of slices through the region of fusion showed that the inner membranes were closely apposed but still distinct (Fig. 3 B, middle; arrowhead; light blue in model panel), indicating that outer NE fusion must precede inner envelope fusion. It is likely that this zygote represents a true intermediate caught just after the initiation of NE fusion, but this state has been observed only once. Because of the rarity of this class, it is formally possible that this image represents an aberrant event in which nuclear fusion had not proceeded normally. Therefore, this issue was examined with an alternative method (see below).

Both the outer and inner membranes were continuous between the two nuclei in 20 tomograms, indicating that NE fusion had been completed at the time of rapid freezing (Figs. 2 C and 4, A–D). In seven of these zygotes, two completely separate and distinct SPBs were observed (Figs. 2 E and 3, A and B), demonstrating that SPB fusion had not yet occurred. In zygotes with separate, unfused SPBs, the median width of the nucleus at

the region of fusion was only 110 nm (measured across the narrowest part of the nucleus between the outer edges of the NE; SD = 30 nm, with one outlier of 302 nm; Fig. 3 C). The narrowness of the isthmus suggests that these zygotes had only just completed nuclear fusion.

The last group of 13 tomograms included zygotes with SPBs in the process of fusion or already fused SPBs (Fig. 4). In all such zygotes, both inner and outer NE fusion was complete. In eight zygotes in the initial or intermediate stages of SPB fusion, the nuclear fusion zone had widened to a median width of 153 nm (SD = 92 nm; one outlier of 1,415 nm; Fig. 3 C). In five zygotes, SPB fusion was either complete or almost complete. In the four zygotes in which the membranes could be measured, the nuclear fusion zone had expanded to a median width of 567 nm (SD = 93 nm). Collectively, these data demonstrate that SPB fusion occurs considerably after the completion of nuclear membrane fusion.

Six layers of the SPB can be detected by ET (O'Toole et al., 1999). The central plaque, which is embedded in the NE, is one of the most electron-dense layers, and this structure was modeled to mark the location of the SPB. Extending from the margin of each SPB is the half-bridge, an electron-dense region of the NE (for review see Jaspersen and Winey, 2004). By ET, the half-bridge is made up of five layers (O'Toole et al., 1999).

Several distinct morphologies of SPBs were seen in cells frozen during the course of nuclear fusion, suggesting that SPB
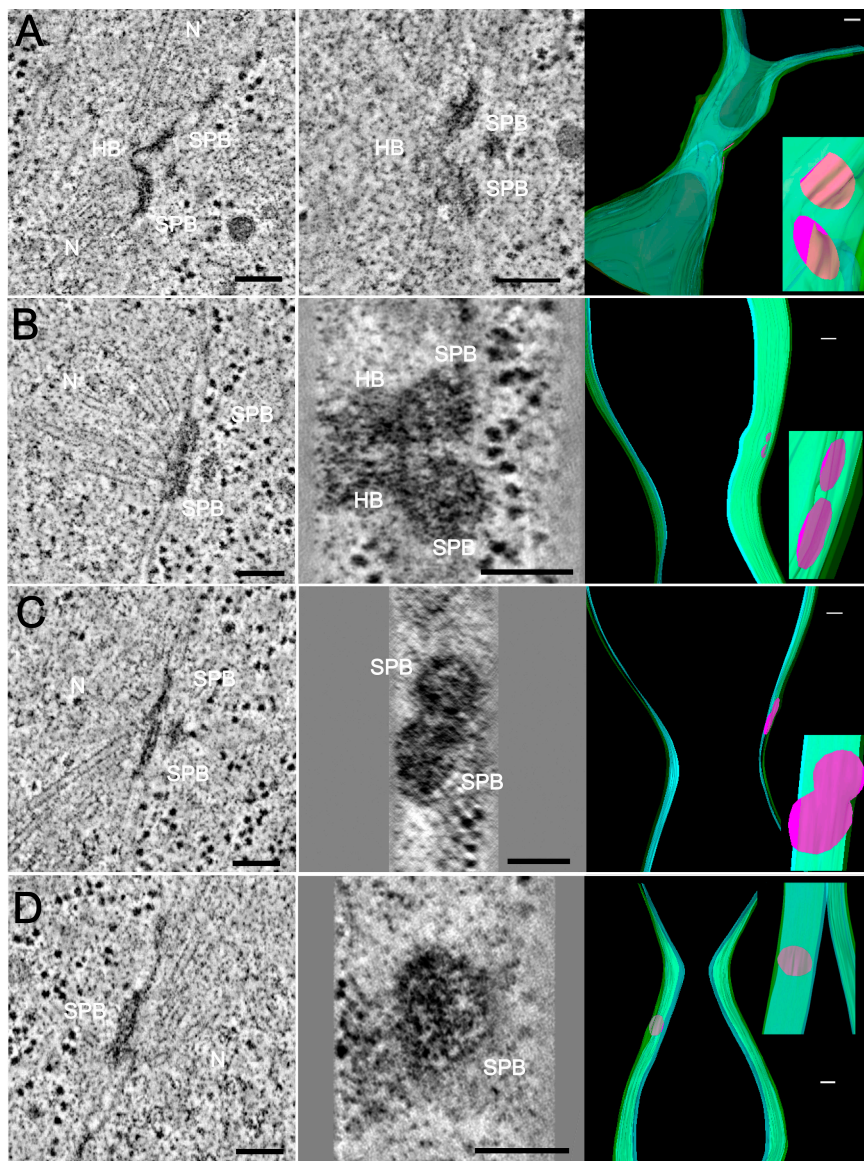
Figure 4. **The stages of SPB fusion.** (A–D) Four stages of SPB fusion are shown, including half-bridge fusion (A), SPBs closely apposed (B), central plaques fusing (C), and fused central plaques (D). The left panel of each row presents a representative slice through the tomogram showing the SPBs in cross section. The middle panel shows magnified images of the SPBs in a partial cross section for A and en face for B–D. The right panels show models indicating the outer and inner NEs (green and light blue, respectively) and the SPB central plaques (pink) at this stage. Insets in model images have been rotated along the y axis to show the SPBs more en face. In A, two half-bridges have joined together, whereas the two central plaques remain distinct. In B, the SPB central plaques are close together but unfused. In C, the central plaques are partially fused. In D, the SPB central plaques have joined together to make a single plaque. In the middle panels, the tomograms were rotated about a z axis centered on the SPBs to make their cross section vertical and were rotated about the y axis to view the SPBs partially or completely en face. HB, half-bridge; N, nucleus; SPB, spindle pole body. Bars, 100 nm.

fusion may occur in several stages. In 8 of the 13 zygotes, the central plaques of the SPBs were clearly separate but joined by their half-bridges. Fig. 4 A shows a representative tomogram in which two central plaques are joined by the multilayered half-bridge. In one zygote, the half-bridges appear to have become joined along their lateral margins; although the central plaques were close together, they had not yet fused (Fig. 4 B). This situation is particularly evident when the SPBs were viewed en face rather than in cross section (Fig. 4 B, middle and inset). In two zygotes, the SPB central plaques appeared to be partially fused (Fig. 4 C). Finally, in two zygotes, we found only a single SPB central plaque, implying that fusion was complete (Fig. 4 D). Based on these observations, a reasonable order for the pathway of SPB fusion would entail interactions first between the half-bridges, most likely via lateral interactions along the half-bridge margin, followed by fusion of the central plaques. Regardless of the detailed pathway of SPB fusion, these results clearly show that SPB fusion occurs as a secondary event and does not initiate NE fusion.

Using fluorescent markers to follow nuclear membrane fusion in live cells

ET is not well suited to distinguish closely spaced temporal events. To complement ET, we developed a method to observe nuclear fusion in live cells using fluorescently tagged proteins as markers for different cellular compartments. To observe SPB congression relative to NE fusion, we initially used Spc42p-RFP to mark the SPB and SS-3XGFP-HDEL to label the lumen of the NE (Fig. 5 and Video 3, available at http://www.jcb.org/cgi/content/full/jcb.200706151/DC1). Spc42p is a key component of the SPB central plaque (Donaldson and Kilmartin, 1996). SS-3XGFP-HDEL is translocated into the lumen of both the NE and ER because of the secretory signal sequence (SS) at its N terminus, and it is retained in the NE/ER by virtue of the C-terminal ER retention signal (HDEL). The signal sequence is cleaved after translocation, so the fluorescing protein will hereafter be referred to as 3XGFP-HDEL. The NE and ER are continuous in yeast; however, the 3XGFP-HDEL signal appears substantially brighter in the NE, as previously observed for
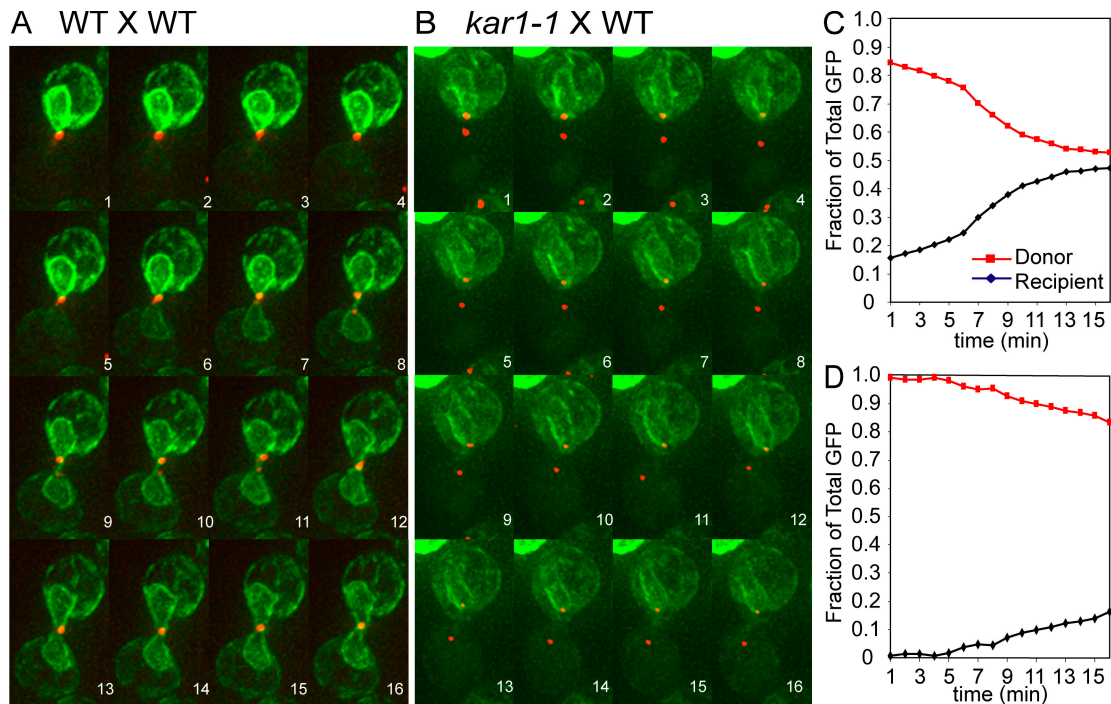
Figure 5. **Transfer of an NE/ER lumenal marker can be used as an indicator of nuclear membrane fusion.** (A) A time-lapse experiment (1-min time points) of two mating yeast cells that have completed cell fusion and are undergoing nuclear fusion. SPB congression has already occurred at the start of the experiment, as indicated by the single spot of Spc42p-RFP fluorescence (red). The NE/ER lumen was visualized using a 3XGFP-HDEL marker (green). After a slow phase of increased fluorescence in the recipient nucleus starting at minute 6, there is a rapid increase in fluorescence in the recipient nucleus. (C) In the graph, a rapid shift in the fraction of total GFP from the donor to the recipient nucleus was initiated at time point 6. Note the separation of SPBs in time points 9–12. (B and D) In a *kar1* nuclear fusion mutant, the slow phase but not the rapid phase of GFP-HDEL transfer was observed. In the *kar1* matings, the two SPBs did not congress (two red dots). WT, wild type.

lumenal proteins (Rose et al., 1989). Data collection was initiated at or soon after cell fusion, as judged by the appearance of the zygotes by differential interference contrast microscopy.

In the example shown in Fig. 5 A, the SPBs were already in close proximity at the beginning of the experiment (t = 1), indicating that nuclear congression had already occurred. Initially, the donor NE was bright, and the acceptor NE was dim. As the experiment progressed, the acceptor NE gradually increased in fluorescence. The initial gradual increase in fluorescence will be referred to as the slow phase of 3XGFP-HDEL transfer. At 6 min after the initial observation, the acceptor NE abruptly increased in fluorescence. The increase in acceptor NE fluorescence was accompanied by a rapid decrease in donor NE fluorescence as the two NEs approached equilibrium. The acceptor reached 50% of the equilibrium value within ∼2.5 min after the onset of the rapid phase of transfer. Concomitant with the rapid phase of 3XGFP-HDEL transfer, the two NEs could be seen to separate at the site of fusion along a line parallel to the axis of the two nuclei, which is indicative of the widening of the nuclear fusion pore (Fig. 5 A, 11-min time point). The transfer of 3XGFP-HDEL from donor to acceptor is quantified in Fig. 5 B based on measurements described in Materials and methods.

Interestingly, in rare examples, such as that shown in Fig. 5 A, the Spc42p-RFP spot formed from the two SPBs was observed to separate into two spots after the NEs had begun to fuse (t = 8). The two Spc42p-RFP spots remained apart until the 12-min time point when they merged, after which they

remained together, even as the NE widened. Thus, the behavior of the Spc42p-RFP in this zygote is consistent with ET, which showed that SPB fusion occurs after NE fusion.

To confirm that the fast phase of the NE luminal filling was caused by NE fusion, we observed 3XGFP-HDEL in matings of karyogamy mutants in which nuclear fusion is blocked. Mutation in the *KAR1* gene causes a block in nuclear congression as a result of defects in the function of the cytoplasmic microtubules (Fig. 5). Nuclear membrane fusion does occur in the rare zygotes of this genotype wherein the nuclei become closely apposed by chance (Rose, 1991). In *kar1-1* X wild-type matings, the two nuclei did not congress, as demonstrated by the presence of two distinct RFP-labeled SPB dots (Fig. 5 B). The acceptor NE showed a gradual increase in fluorescence intensity but never a transition to the rapid phase of 3XGFP-HDEL transfer (Fig. 5 D and not depicted). The GFP fluorescence in the donor NE remained considerably brighter than the acceptor NE throughout the course of the experiment. Given the dependence of the rapid 3XGFP-HDEL transfer on proteins required for karyogamy and the temporal correlation of this transfer with the onset of NE expansion, we conclude that the rapid phase of transfer is indicative of the onset of NE fusion. Most likely, the rapid phase of transfer corresponds to the dilation of the membrane fusion pore. We surmise that the slow phase of 3XGFP-HDEL transfer is caused by the recycling of HDEL-bearing proteins from the Golgi to the NE/ER of both parents. Although this introduces a small amount of background fluorescence, a
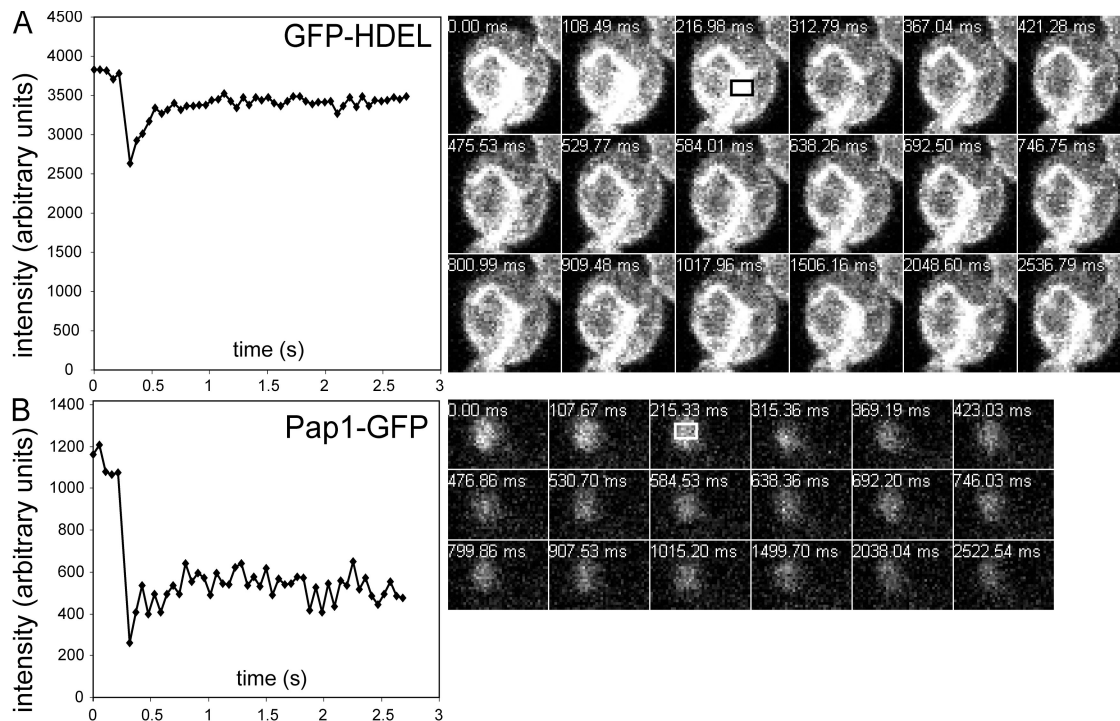
Figure 6. FRAP analysis using 3XGFP-HDEL and Pap1-GFP. (A and B) FRAP analysis was performed on cells expressing either 3XGFP-HDEL (A) or Pap1-GFP (B). The graphs show the initial fluorescence intensity in the ROIs in five images, a rapid drop in fluorescence intensity in the bleached area, and recovery of fluorescence intensity in the bleached area. Three prebleach images are shown, with the area to be bleached indicated by a rectangle in the last prebleach image. Representative postbleach recovery images are shown from the time course, lasting just under 3 s.

sharp transition between the slow and rapid phases could be readily discerned in almost all zygotes.

Direct tests of the nuclear fusion models using live cell microscopy

Transfer of lumenal 3XGFP-HDEL to the acceptor NE/ER is indicative of outer NE fusion, but it does not provide information about the last step of NE fusion, the fusion of the inner nuclear membranes. In principle, this may occur either at the same time as outer membrane fusion as part of a single concerted reaction or as a temporally distinct event. To reveal inner nuclear membrane fusion, we developed an assay based on the transfer of a nucleoplasmic marker from a donor nucleus to an acceptor nucleus. We tested several nucleoplasmic markers, including NLS-tagged fluorescent proteins, fluorescent protein–tagged histones, and fluorescent protein–tagged poly (A) polymerase. NLS-CFP and -YFP exhibited high levels of background cytoplasmic localization as well as rapid transfer into unfused nuclei, presumably because of rapid shuttling between the nucleus and cytoplasm (Damelin and Silver, 2000 and our unpublished data). Fluorescent protein–tagged histones exhibited very low cytoplasmic background and no observable transfer between unfused nuclei. However, fluorescent chromatin from the two haploid nuclei remained segregated as distinct domains in the newly formed diploid nucleus (unpublished data), which obscured attempts to determine a precise time for the completion of nuclear fusion. Ultimately, fluorescent protein–tagged poly (A) polymerase (Pap1p) was found to be suitable for our studies. Fluorescent protein–tagged Pap1p showed both a low

cytoplasmic background and a uniform distribution within the nucleus, presumably because its diffusion is not limited by stable association with nuclear polymers (Lingner et al., 1991a).

We used FRAP to determine whether there were fundamental differences in the rate of diffusion between 3XGFP-HDEL and fluorescent protein–tagged Pap1p fusions that might cause differences in their observed rates of transfer. In this technique, a small region of the cell containing the fluorescent protein was bleached, and the bleached area was monitored for recovery of the fluorescent signal. The rate of diffusion can be measured from the rate of fluorescence recovery. For these experiments, we performed FRAP analysis on 3XGFP-HDEL and Pap1p-GFP. Pap1p-GFP was used instead of the Pap1p-RFP or Pap1p-mCherry (monomeric Cherry fluorescent protein) constructs used in the time course experiments because the RFPs were difficult to bleach with available laser lines. However, GFP and RFP diffusion rates have been previously shown to be very similar (Nolan et al., 2006). Thus, any substantial differences in the behaviors of fluorescent protein–tagged Pap1p and 3XGFP-HDEL would be the result of differences in the Pap1p and HDEL portions of the chimeras. We found that Pap1p-GFP and 3XGFP-HDEL exhibited similar rates of recovery (Fig. 6), with Pap1p-GFP diffusing somewhat faster than 3XGFP-HDEL (mean $t_{1/2} = 0.16$ s [$n = 18$] vs. 0.22 s [$n = 20$], respectively). Thus, any delay observed for fluorescent protein–tagged Pap1p relative to 3XGFP-HDEL would likely underestimate the true difference. The recovery of Pap1-GFP and 3XGFP-HDEL averaged 97% and 96%, respectively, taking into account the reduced pool of unbleached fluorescent protein.

Figure 7. **Transfer of the NE/ER luminal marker can be detected before nucleoplasmic mixing.** (A) A time-lapse experiment after the transfer of 3XGFP-HDEL and the reciprocal transfer of Pap1-RFP in wild-type mating cells at 1-min intervals. Note the filling of the recipient NE lumen in time point 5 (green-bordered panel), whereas visible transfer of the nucleoplasmic marker does not occur until time point 6 (red-bordered panel). (B) The fraction of total GFP and RFP in the donor and recipient nuclei over time. The initial time of GFP transfer was determined from the intersection between the slopes of the slow and rapid phases of transfer, occurring at 4 min in this example. The initial phase of RFP transfer was determined similarly, occurring ∼30 s after GFP transfer. The initial times are indicated by dotted lines on the graph. (C and D) Two representative graphs from time-lapse experiments using 30-s and 20-s time points, respectively. In these particular experiments, Pap1-mCherry was used instead of RFP. Note that initiation of the rapid transfer of GFP from the donor to the recipient was detected before rapid transfer of the nucleoplasmic marker (indicated by dotted lines on graph). (E) A histogram of the difference between the initial times of transfer measured for GFP and RFP/mCherry observed using time-lapse microscopy ($n = 47$). FP, fluorescent protein.
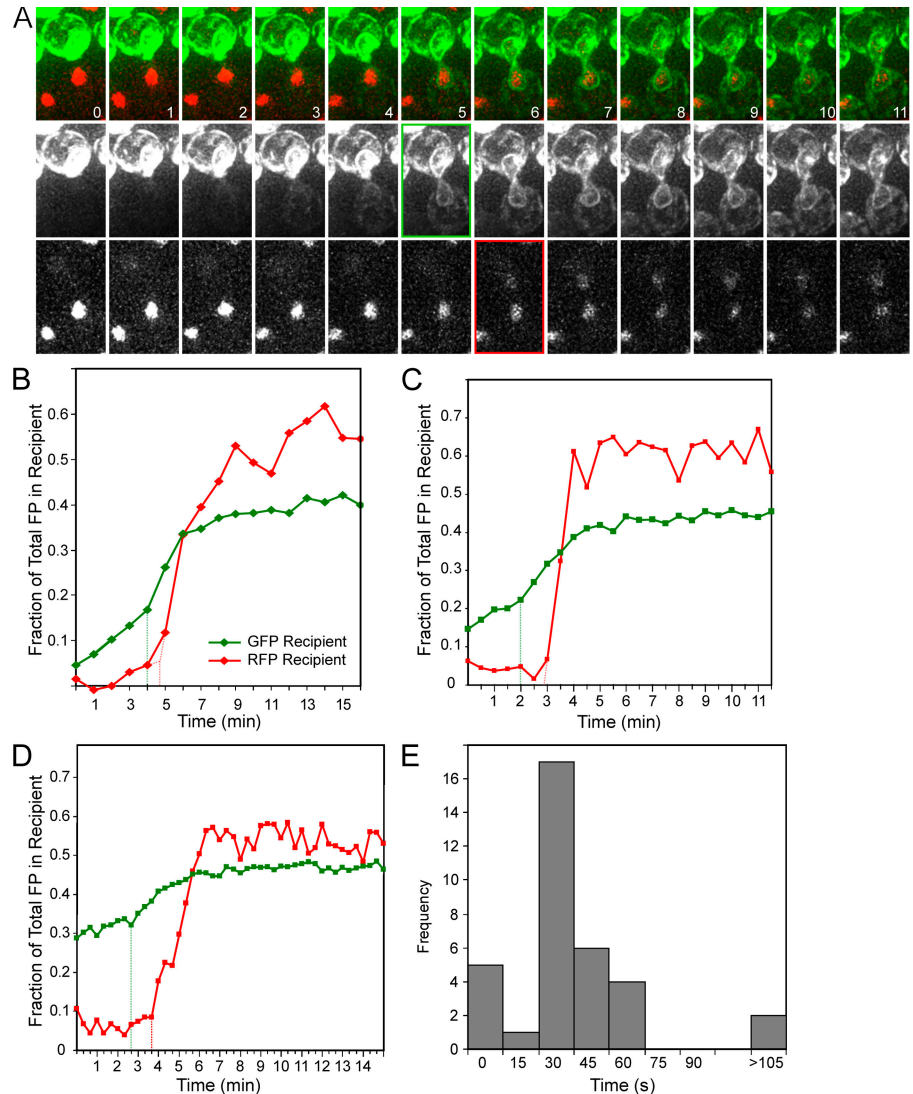
After establishing that there were no substantial differences in the diffusion rates of the marker proteins, we performed time-lapse microscopy of zygotes in which both proteins were present. Cells of one mating type were labeled with 3XGFP-HDEL and mated with cells of the opposite mating type labeled with Pap1p-RFP or Pap1p-mCherry (Fig. 7). A total of 47 zygotes were imaged, with images taken every 1 min, 30 s, or 20 s. In each, the fluorescence intensity was measured on equivalent areas of the donor and recipient and corrected for background fluorescence using a region outside the cell. Photobleaching during the course of the experiment was corrected by fitting the measurements to a first-order exponential.

In the zygote shown in Fig. 7, the shift from the slow phase to the rapid phase of 3XGFP-HDEL transfer occurred at ∼5 min, reaching a half-maximal transfer within 2 min (Fig. 7 B). In contrast, the first time point in which a considerable amount of Pap1-RFP fluorescence was observed in the recipient nucleus was at 6 min. Extrapolation of the initial slope to the x axis suggested that transfer initiated at ∼5.5 min, reaching half-maximal transfer at ∼7 min. Subsequent experiments in which images were acquired every 20 or 30 s provided greater temporal re-

solution of the two fusion events (Fig. 7, C and D). Out of the 47 zygotes examined, 32 exhibited clear temporal separations between the initiation times of marker protein transfer, and five showed no measurable delay (Fig. 7 E). The remaining 10 zygotes were not interpretable because the transfer had begun before beginning the observation, transfer did not occur during the observation period, or the shift from the slow to rapid phase of 3XGFP-HDEL transfer was not sufficiently pronounced to determine the time of initiation. As expected, the number of zygotes in which a temporal delay could not be discerned was dependent on the density of time points (3/13 for 1 min, 1/10 for 20 s, and 1/14 for 30 s experiments). The median time for all 37 interpretable zygotes was 30 s (40 s for the 10 zygotes imaged at 20-s intervals). Two of the zygotes examined using 20-s time points showed unusually long delays in the time of initiation of Pap1p-mCherry transfer relative to 3XGFP-HDEL transfer (440 and 620 s). Because the more rapid time point experiments necessitated increased exposure to the excitation light, these may represent photodamaged cells. When these two cells were omitted from the analysis, the mean time delay for the 20-s interval image sets was 31.25 s and for all image sets was 29 s ($n = 35$; SD = 17).

We conclude that inner NE fusion occurs after outer NE fusion in two distinct membrane fusion events. Taking these data together with the ET, we conclude that nuclear fusion occurs in three steps, culminating in the formation of a diploid nucleus with a single fused SPB.

Discussion

In this study, both ET and live cell microscopy were used to examine the details of nuclear fusion during yeast conjugation. ET revealed several nuclear morphologies consistent with nuclei poised at various intermediate stages of nuclear fusion, including outer membrane fusion, inner membrane fusion, SPB satellite/bridge fusion, and SPB fusion. In one example, outer membrane fusion was observed without inner membrane fusion, suggesting that outer membrane fusion precedes inner nuclear membrane fusion. In addition, consistent with the hypothesis that nuclear membrane fusion precedes SPB fusion, complete nuclear membrane fusion was observed in zygotes that still had distinct SPB central plaques. Apparent intermediates in SPB fusion were seen in zygotes with expanded nuclear fusion pores, indicating that SPB fusion occurs considerably later than nuclear membrane fusion. By live cell microscopy, initiation of the transfer of a luminal NE marker was detected ~30 s before transfer of a nucleoplasmic marker, indicating that outer membrane fusion precedes inner membrane fusion. Collectively, these data demonstrate that budding yeast nuclear fusion occurs in at least three distinct stages.

The role of the half-bridge in SPB fusion
The observation of nuclear membrane fusion before SPB fusion was surprising given a previous study suggesting that fusion of the SPB plaques is the initial event, occurring simultaneously with nuclear membrane fusion (Byers and Goetsch, 1975). It is likely that the differences between these studies are the result of both the reliability of rapid freezing as a way to immobilize cellular events with high structural precision and the greater 3D resolution of ET. Initial fusion intermediates comprise as little as 5 nm of membrane length in a 2D view and, thus, could easily have been missed by techniques dependent on serial sectioning.

Both our work and a previous study have shown the key role of SPB half-bridges in the fusion process (Byers and Goetsch, 1975). The half-bridges are the sites of nucleation for the cytoplasmic microtubules that pull the nuclei together for fusion during mating. As a result, the half-bridges become located adjacent to the site of nuclear membrane fusion, whereas the central plaques are initially more peripheral. From our data (Fig. 4) and previous work (Byers and Goetsch, 1975), SPB fusion appears to initiate along the lateral edge of the half-bridge, culminating in side by side fusion of the central plaques. Note that the original one-step model required that the two SPBs be in one specific orientation at the end of congression to allow their fusion along their lateral edges. However, a substantial flaw of the model was that it did not provide a mechanism to ensure that the two SPBs would be properly aligned about the axis of the cytoplasmic microtubules. In the three-step model, the SPBs become coplanar within the NE before their fusion, with the half-bridges roughly proximal to each other. After move-

ment together within the plane of the NE, SPB fusion would then necessarily occur along their lateral margins.

Recently, the half-bridge has been shown to be composed, in part, of a parallel assembly of a conserved, centrin-binding, centrosomal protein Sfi1p (Li et al., 2006). The Sfi1p molecules in this assembly are arranged with their N termini next to the SPB and their C termini extending outward, providing polarity to the overall structure of the half-bridge (Li et al., 2006). The inherent polarity of Sfi1p in the half-bridge may provide a mechanism for orienting the association between the two SPBs. Lateral association of Sfi1p filaments would serve to align the initially randomly oriented SPBs within the plane of the NE, assuring that the two SPB central plaques fuse into a single diploid SPB.

The final step in SPB fusion entails a third membrane fusion event, when the two central plaques coalesce into a single plaque. The central plaques are embedded in the NE similar to nuclear pores, with the inner and outer membranes joined at the edges. As the two plaques come together, topological considerations dictate that the inner and outer membranes must pinch together and fuse to allow the two SPBs to form into one. It is possible that proteins associated with the half-bridge aid in this late stage or in the earlier formation of the nuclear fusion pore. During SPB duplication, the bridge is thought to play a role in facilitating the membrane embedment of the nascent SPB (for review see Jaspersen and Winey, 2004), which must involve fusion of the inner and outer nuclear membrane to form a pore in the NE.

Details of nuclear fusion revealed by ET and live cell microscopy
Although ET captured only static views of intermediates in nuclear fusion, live cell microscopy permitted the observation of nuclear fusion in real time. Whereas short-lived intermediates are only rarely sampled and difficult to identify by static imaging, all live cells would necessarily transit through the intermediate stage, however short their duration. Considering the events of NE fusion, the initiation of transfer of Pap1-mCherry or -RFP occurred ~30 s after 3XGFP-HDEL (Fig. 7). The overall time course of nuclear fusion after cell fusion is ~10–15 min (Maddox et al., 1999; and this study), predicting that zygotes in which outer NE fusion but not inner NE fusion had occurred should be very rare. Consistent with this prediction, only one such zygote was observed by ET out of a total of 22 examined.

Conversely, live cell imaging does not yet provide sufficient spatial resolution to detect the detailed events of SPB fusion. Remarkably, in a few cases, the two SPBs were observed to separate and rejoin after membrane fusion, confirming the results from ET that SPB fusion occurs only later. The live cell imaging also suggests that the SPBs have considerable freedom of movement within the plane of the membrane before fusion. Free movement and rotation would likely be necessary to allow the two haploid SPBs to align for proper fusion to form a single diploid SPB. These results also confirm that during mating, the SPB has a remarkable level of plasticity to allow fusion of two distinct structures into one single diploid SPB.

FRAP confirmed that the temporal order was not simply the result of different rates of fluorescent protein diffusion. The half-time of recovery for Pap1p-GFP was somewhat faster

Table I. **Strains and plasmids**

Strain	Genotype	Source or reference
MS23	MATα, trp1-Δ1, lys2-801, ade2-101	Rose laboratory
MS1554	MATa, ura3-52, leu2-3,112, ade2-101, his3-Δ200	Rose laboratory
MS740	MATα, leu2-3,112, ura3-52, ade2-101, kar1-1	Rose laboratory
MS7814	Same as MS740 except SPC42:mRFP	This study
MS1686	MATα, his3-Δ200, ura3-52, leu2-3,112, ade2-101, trp1-Δ1	Rose laboratory
MS7816	Same as MS1686 except PAP1:mRFP	This study
MS1691	MATa, his3-Δ200, ura3-52, leu2-3,112, ade2-101, trp1-Δ1	Rose laboratory
MS7818	Same as MS1691 except pMR5029	This study
MS7728	Same as MS1691 except SPC42:mRFP	This study
MS7748	Same as MS7728 except SS-3XGFP-HDEL (TRP1)	This study
MS2290	MATα, his3-Δ200, ura3-52, leu2-3,112, trp1-Δ1	Rose laboratory
MS7840	Same as MS7840 except PAP1:mCherry	This study
MS7848	Same as MS1691 except PAP1:GFP	This study
Plasmid	**Relevant markers**	**Source or reference**
pMR5029	SS-3XGFP-HDEL in pRS414 (TRP1)	N. Erdeniz, Rose laboratory
pMR5484	pFa6a-mRFP-kanMX6	S. Clark and R. Tsien
pMR5597	pFa6a-mCherry-kanMX6	S. Clark and R. Tsien

than 3XGFP-HDEL (mean $t_{1/2}$ = 0.16 s vs. 0.22 s, respectively). Similarly, the rate of transfer from the donor nucleus to the recipient nucleus was substantially faster for the Pap1p hybrids than for 3XGFP-HDEL. The slower transfer of the earlier transferring protein would lead to an underestimate of the time delay, reinforcing the conclusion that the two events are temporally distinct. However, in each case, the half-time of transfer (1–2 min) was also many times slower than the half-time of recovery after photobleaching. Unlike FRAP, the rate of transfer between the nuclear compartments is likely to be impeded by the geometry of the fusion pore connecting them. Similar effects have been observed on the transfer of cytoplasmic proteins during cell fusion (Nolan et al., 2006).

Phenotypic analysis using newly defined nuclear fusion stages

Given that nuclear fusion occurs in multiple steps, it is likely that the *kar* mutations that block NE fusion may affect different steps. For example, it should now be possible to distinguish karyogamy mutants that are proficient in outer membrane fusion yet deficient in inner membrane fusion. The possibility that some mutations block inner NE fusion might explain why most mutations blocking NE fusion affect components localized within the lumen of the NE. Mutations affecting outer NE fusion have been harder to find, possibly because of effects on the secretory pathway as well. Similarly, mutants may be identified that complete nuclear membrane fusion but block at some stage of SPB fusion, provided these mutants are not also impaired in congression.

Collectively, these data permit a rather detailed description of nuclear fusion in the budding yeast. NE fusion occurs in two steps followed by SPB fusion, which is consistent with the predictions of the three-step model. However, ET suggests that SPB fusion also occurs in several steps. The two SPBs must move together within the plane of the NE followed by lateral association of the half-bridges, culminating in the merger of the central plaques. Future studies will address how outer NE- and/or SPB-associated proteins facilitate the initiation of nuclear and SPB fusion.

Materials and methods

Strains and yeast methods
All strains used in this study are listed in Table I. Yeast media was prepared, and general methodology was followed as described previously (Rose et al., 1990; Amberg et al., 2005). Genomic integrations of GFP, monomeric RFP (mRFP), and mCherry fluorescent tags at the C terminus of *PAP1* and *SPC42* were conducted using previously published vectors and methods (Longtine et al., 1998). R.Y. Tsien (University of California, San Diego, San Diego, CA) provided the mCherry and mRFP fluorescent tags, S. Clark (Princeton University, Princeton, NJ) provided mRFP and mCherry kanMX constructs, and N. Erdeniz (Princeton University) provided the SS-3XGFP-HDEL construct. The *SPC42*-mRFP was fully functional and supported normal rates of growth and nuclear fusion. In brief, primers were designed to amplify the integration cassette, adding ∼40 base pairs of homology to the chromosomal region of interest at either end of the fragment to facilitate integration. PCR products were pooled and gel purified. Then, the strain of interest was transformed. Transformants were checked for proper integration using a diagnostic PCR. Existing GFP integration cassettes were modified for mRFP (pMR5484) and mCherry (pMR5597) integration by the same method using the same primers. During the course of the study, RFP constructs were replaced with mCherry constructs because of the improved stability of this red fluorescent marker (Shaner et al., 2005).

Preparing mating mixtures for ET
Individual liquid cultures of MATα and MATa strains were prepared and mated together as described previously (Gammie and Rose, 2002). For ET, mating mixtures were mated on a nitrocellulose filter disk for 2.5 h at 30°C. Cells were prepared for electron microscopy as reported previously (O'Toole et al., 2002; Yoder et al., 2005). In brief, mating cells were resuspended in liquid medium, collected by centrifugation, frozen under high pressure, and subsequently freeze substituted in acetone containing 2% osmium tetroxide and 0.1% uranyl acetate at –90°C for 3 d. Cells were subsequently warmed to –20°C for 12 h, rinsed in acetone, warmed to room temperature over 2 h, and embedded in epoxy resin. Serial semithick sections (200–300 nm) were cut using a microtome (Reichert Ultracut-E; Leica), collected on Formvar-coated slot grids, and stained with aqueous uranyl acetate and Reynolds lead citrate. 15-nm colloidal gold particles (Sigma-Aldrich) were applied to both surfaces of the sections to use as fiducial markers during image alignment.

Electron microscopy, tomography reconstruction, and modeling
ET was conducted as described previously (O'Toole et al., 2002). In brief, sections were placed in a high-tilt specimen holder (Gatan), and images were recorded using a Tecnai TF20 or TF30 intermediate voltage electron microscope (FEI) operated at 200 kV or 300 kV, respectively. Using a rotating sample holder, electron microscopy images were captured every 1° over a ±60° range using a CCD camera (2K by 2K; Gatan). To collect dual-axis datasets, the grid was rotated 90°, and a second tilt series was

collected. Tomography reconstructions were calculated, displayed, and analyzed using the IMOD software package (Kremer et al., 1996). The single-axis tomograms were aligned to each other and combined to create a single tomogram (Mastronarde, 1997). Objects such as microtubules, outer and inner NEs, and SPBs were modeled on the tomography reconstructions using the same software. 21 tomograms and models of wild-type mating yeast cells were generated. Nuclear fusion pore dilation was measured using IMOD software. Measurements were taken between the outer envelopes at the narrowest point in the zone of fusion.

Live cell microscopy data collection and analysis
For live cell microscopy, mating mixtures were prepared as described previously (Gammie and Rose, 2002). However, instead of transferring mating mixtures to a nitrocellulose filter, cells were immediately transferred to a 2% agarose pad (in synthetic complete media) on a microscope slide and incubated at RT for 1.5 h before data collection.

Time-lapse microscopy was conducted using a microscopy system (DeltaVision; Applied Precision) based on an inverted microscope (TE200; Nikon) and a CCD camera (CoolSNAP HQ; Photometrics). For all images, a 100× NA 1.4 Apochromat oil immersion objective (Nikon) was used. At various time points, a GFP image (FITC filter set) and an mCherry/RFP image (rhodamine filter set) were captured at 0.5-μm intervals for a 10-section z stack. Images were deconvolved using the constrained iterative program in softWoRx (Applied Precision). Images were prepared for publication with Photoshop (Adobe) using linear contrast and intensity adjustments. Where necessary, image size was increased using bicubic resampling. Time-lapse experiments successfully capturing zygotes before, during, and after nuclear fusion as judged by 3XGFP-HDEL transfer were analyzed. Zygotes with a weak 3XGFP-HDEL signal or zygotes too early or too late in nuclear fusion were not analyzed further. By these criteria, ∼50% of the zygotes were unusable. GFP and mCherry/RFP fluorescence in donor and recipient cells was analyzed on the deconvolved images using ImageJ (National Institutes of Health). For each time point, the mean fluorescence intensity was determined for a region of interest (ROI) encompassing the donor nucleus. Equal-sized ROIs encompassing the recipient nucleus and neighboring background areas of the slide were also measured. The integrated fluorescence intensity was calculated and corrected first for background signal and then for photobleaching using a simple first-order exponential decay model. The corrected integrated intensities for donor and recipient were expressed and graphed as the fraction of total fluorescence, taking the sum of the donor and recipient ROIs as 100%. 3XGFP-HDEL transfer was biphasic, with a slow transfer phase followed by a rapid transfer during nuclear fusion. The initial time of transfer during nuclear fusion was determined from the intersection of the slopes of the slow and rapid phases, interpolating between time points when necessary. mCherry and RFP transfer typically occurred in a single phase of rapid transfer, with little or no signal in the recipient nucleus before the transfer. Therefore, the initial period of transfer was taken from the intersection of the slope with the x intercept.

FRAP
FRAP analysis on 3XGFP-HDEL and Pap1-GFP was performed using a confocal system (LSM510; Carl Zeiss, Inc.) housed in the Microscopy Core Facility of Princeton University (Department of Molecular Biology). Five prebleach images were collected followed by a four to six iteration photobleach and immediate collection of 45 postbleach images (30–100 ms apart depending on the experiment). 3XGFP-HDEL was bleached using 488- and 514-nm laser lines at 95% power with the bleach set at 100%. Pap1-GFP was bleached using the 488-nm laser line at 95% power with the bleach set at 80%. The half-time of recovery was determined using a MATLAB program written by T. Gregor (Princeton University, Princeton, NJ). The mean recovery for Pap1-GFP and 3XGFP-HDEL (97% and 96%, respectively) was determined by measuring the fraction of total nuclear fluorescence in the ROI before and after the photobleach. For example, in the experiment shown in Fig. 6 B, the total nuclear fluorescence at t = 0 was ∼4,000 U, which was reduced to ∼2,200 U by bleaching. The total fluorescence of the ROI was ∼1,100 U before the bleaching, which recovered to ∼600 U. Thus, the ROI contained ∼27.5% of the total nuclear fluorescence before the bleach and ∼27.3% of the total nuclear fluorescence after recovery, indicating nearly 100% recovery.

Online supplemental material
Videos show slices through a tomogram (Video 1), a 3D model of a wild-type zygote (Video 2), and transfer of 3X-GFP-HDEL during nuclear fusion in live cells (Video 3). Table S1 lists all tomographic reconstructions ordered by stage. Online supplemental material is available at http://www.jcb.org/cgi/content/full/jcb.200706151/DC1.

References

Amber, D.C., D. Burke, and J. Strathern. 2005. Methods in Yeast Genetics: a Cold Spring Harbor Laboratory Course Manual. Cold Spring Harbor Laboratory, Cold Spring Harbor, NY. 230 pp.

Beh, C.T., V. Brizzio, and M.D. Rose. 1997. KAR5 encodes a novel pheromone-inducible protein required for homotypic nuclear fusion. *J. Cell Biol.* 139:1063–1076.

Beilharz, T., B. Egan, P.A. Silver, K. Hofmann, and T. Lithgow. 2003. Bipartite signals mediate subcellular targeting of tail-anchored membrane proteins in *Saccharomyces cerevisiae*. *J. Biol. Chem.* 278:8219–8223.

Brizzio, V., W. Khalfan, D. Huddler, C.T. Beh, S.S.L. Andersen, M. Latterich, and M.D. Rose. 1999. Genetic interactions between KAR7/SEC71, KAR8/JEM1, KAR5, KAR2 during nuclear fusion. *Mol. Biol. Cell.* 10:609–626.

Byers, B. 1981a. Cytology of the yeast life cycle. *In* The Molecular Biology of the Yeast *Saccharomyces*: Life Cycle and Inheritance. J.N. Strathern, E.W. Jones, and J.R. Broach, editors. Cold Spring Harbor Laboratory, Cold Spring Harbor, NY. 59–96.

Byers, B., and L. Goetsch. 1974. Duplication of spindle plaques and integration of the yeast cell cycle. *Cold Spring Harb. Symp. Quant. Biol.* 38:123–131.

Byers, B., and L. Goetsch. 1975. Behavior of spindles and spindle plaques in the cell cycle and conjugation of *Saccharomyces cerevisiae*. *J. Bacteriol.* 124:511–523.

Catlett, N.L., and L.S. Weisman. 2000. Divide and multiply: organelle partitioning in yeast. *Curr. Opin. Cell Biol.* 12:509–516.

Chen, E.H., and E.N. Olson. 2005. Unveiling the mechanisms of cell-cell fusion. *Science.* 308:369–373.

Damelin, M., and P.A. Silver. 2000. Mapping interactions between nuclear transport factors in living cells reveals pathways through the nuclear pore complex. *Mol. Cell.* 5:133–140.

Donaldson, A.D., and J.V. Kilmartin. 1996. Spc42p: a phosphorylated component of the *S. cerevisiae* spindle pole body (SPB) with an essential function during SPB duplication. *J. Cell Biol.* 132:887–901.

Gammie, A.E., and M.D. Rose. 2002. Assays of cell and nuclear fusion. *Methods Enzymol.* 351:477–498.

Gammie, A.E., V. Brizzio, and M.D. Rose. 1998. Distinct morphological phenotypes of cell fusion mutants. *Mol. Biol. Cell.* 9:1395–1410.

Jaspersen, S.L., and M. Winey. 2004. The budding yeast spindle pole body: structure, duplication, and function. *Annu. Rev. Cell Dev. Biol.* 20:1–28.

Kremer, J.R., D.N. Mastronarde, and J.R. McIntosh. 1996. Computer visualization of three-dimensional image data using IMOD. *J. Struct. Biol.* 116:71–76.

Kurihara, L.J., C.T. Beh, M. Latterich, R. Schekman, and M.D. Rose. 1994. Nuclear congression and membrane fusion: two distinct events in the yeast karyogamy pathway. *J. Cell Biol.* 126:911–923.

Latterich, M., and R. Schekman. 1994. The karyogamy gene *KAR2* and novel proteins are required for ER-membrane fusion. *Cell.* 78:87–98.

Li, S., A.M. Sandercock, P. Conduit, C.V. Robinson, R.L. Williams, and J.V. Kilmartin. 2006. Structural role of Sfi1p-centrin filaments in budding yeast spindle pole body duplication. *J. Cell Biol.* 173:867–877.

Lingner, J., J. Kellermann, and W. Keller. 1991a. Cloning and expression of the essential gene for poly (A) polymerase from *S. cerevisiae*. *Nature.* 354:496–498.

Longtine, M.S., A. McKenzie III, D.J. Demarini, N.G. Shah, A. Wach, A. Brachat, P. Philippsen, and J.R. Pringle. 1998. Additional modules for versatile and economical PCR-based gene deletion and modification in *Saccharomyces cerevisiae*. *Yeast.* 14:953–961.

Maddox, P., E. Chin, A. Mallavarapu, E. Yeh, E.D. Salmon, and K. Bloom. 1999. Microtubule dynamics from mating through the first zygotic division in the budding yeast *Saccharomyces cerevisiae*. *J. Cell Biol.* 144:977–987.

Marsh, L., and M.D. Rose. 1997. The pathway of cell and nuclear fusion during mating in *S. cerevisiae*. *In* The Molecular and Cellular Biology of the Yeast *Saccharomyces*. Vol. 3. J.R. Broach, J.R. Pringle, and E.W. Jones, editors. Cold Spring Harbor Laboratory, Cold Spring Harbor, NY. 827–888.

Mastronarde, D.N. 1997. Dual-axis tomography: an approach with alignment methods that preserve resolution. *J. Struct. Biol.* 120:343–352.

Meeusen, S., J.M. McCaffery, and J. Nunnari. 2004. Mitochondrial fusion intermediates revealed in vitro. *Science*. 305:1747–1752.

Molk, J.N., E.D. Salmon, and K. Bloom. 2006. Nuclear congression is driven by cytoplasmic microtubule plus end interactions in *S. cerevisiae*. *J. Cell Biol.* 172:27–39.

Ng, D.T.W., and P. Walter. 1996. ER membrane protein complex required for nuclear fusion. *J. Cell Biol.* 132:499–509.

Nishikawa, S., and T. Endo. 1997. The Yeast JEM1p is a DnaJ-like protein of the endoplasmic reticulum membrane required for nuclear fusion. *J. Biol. Chem.* 272:12889–12892.

Nishikawa, S., S.W. Fewell, Y. Kato, J.L. Brodsky, and T. Endo. 2001. Molecular chaperones in the yeast endoplasmic reticulum maintain the solubility of proteins for retrotranslocation and degradation. *J. Cell Biol.* 153:1061–1069.

Nishikawa, S., Y. Terazawa, T. Nakayama, A. Hirata, T. Makio, and T. Endo. 2003. Nep98p is a component of the yeast spindle pole body and essential for nuclear division and fusion. *J. Biol. Chem.* 278:9938–9943.

Nolan, S., A.E. Cowan, D.E. Koppel, H. Jin, and E. Grote. 2006. FUS1 regulates the opening and expansion of fusion pores between mating yeast. *Mol. Biol. Cell*. 17:2439–2450.

O'Toole, E.T., M. Winey, and J.R. McIntosh. 1999. High-voltage electron tomography of spindle pole bodies and early mitotic spindles in the yeast *Saccharomyces cerevisiae*. *Mol. Biol. Cell*. 10:2017–2031.

O'Toole, E.T., M. Winey, J.R. McIntosh, and D.N. Mastronarde. 2002. Electron tomography of yeast cells. *Methods Enzymol*. 351:81–95.

Ogle, B.M., M. Cascalho, and J.L. Platt. 2005. Biological implications of cell fusion. *Nat. Rev. Mol. Cell Biol.* 6:567–575.

Okamoto, K., and J.M. Shaw. 2005. Mitochondrial morphology and dynamics in yeast and multicellular eukaryotes. *Annu. Rev. Genet.* 39:503–536.

Rose, M.D. 1991. Nuclear fusion in yeast. *Annu. Rev. Microbiol.* 45:539–567.

Rose, M.D. 1996. Nuclear fusion in the yeast, *Saccharomyces cerevisiae. Annu. Rev. Cell Dev. Biol.* 12:663–695.

Rose, M.D., and G.R. Fink. 1987. KAR1, a gene required for function of both intranuclear and extranuclear microtubules in yeast. *Cell*. 48:1047–1060.

Rose, M.D., L.M. Misra, and J.P. Vogel. 1989. *KAR2*, a karyogamy gene, is the yeast homolog of the mammalian BiP/GRP78 gene. *Cell*. 57:1211–1221.

Rose, M.D., F. Winston, and P. Hieter. 1990. Methods in Yeast Genetics: a Cold Spring Harbor Laboratory Course Manual. Cold Spring Harbor Laboratory, Cold Spring Harbor, NY. 198 pp.

Shaner, N.C., P.A. Steinbach, and R.Y. Tsien. 2005. A guide to choosing fluorescent proteins. *Nat. Methods*. 2:905–909.

Sprague, G.F., Jr., and J.W. Thorner. 1992. Pheromone response and signal transduction during the mating process of *Saccharomyces cerevisiae*. *In* The Molecular and Cellular Biology of the Yeast *Saccharomyces*. Vol. 2. J.R. Broach, J.R. Pringle, and E.W. Jones, editors. Cold Spring Harbor Laboratory, Cold Spring Harbor, NY. 657–744.

White, J.M., and M.D. Rose. 2001. Yeast mating: getting close to membrane merger. *Curr. Biol.* 11:R16–R20.

Yoder, T.J., M.A. McElwain, S.E. Francis, J. Bagley, E.G.D. Muller, B. Pak, E.T. O'Toole, M. Winey, and T.N. Davis. 2005. Analysis of a spindle pole body mutant reveals a defect in biorientation and illuminates spindle forces. *Mol. Biol. Cell*. 16:141–152.